Drug Design, Development and Therapy

Dovepress
open access to scientific and medical research

Open Access Full Text Article

ORIGINAL RESEARCH

RGD-Conjugated Resveratrol HSA Nanoparticles as a Novel Delivery System in Ovarian Cancer Therapy

This article was published in the following Dove Press journal:
Drug Design, Development and Therapy

Qifang Long
Weipei Zhu
Liangsheng Guo
Li Pu

Department of Gynecology and Obstetrics, The Second Affiliated Hospital of Soochow University, Suzhou, People's Republic of China

Background: To establish a novel delivery system of RGD-conjugated resveratrol human serum albumin (HAS) nanoparticles in ovarian cancer therapy.

Methods: The nanoparticles system was characterized for physicochemical properties, the stability in the serum and in vitro release. The comparison between RVT injection, HSA-RVT NPs and RGD-HSA-RVT NPs regarding tissue distributions and pharmacokinetics was also carried out using mice as the animal models.

Results: The results showed that RGD-HSA-RVT NPs were characterized of small particle size about 128.2 nm and negative zeta potential about −21.42 mV, and drug controlled to release slowly on a biphasic pattern. Compared with control groups, RGD-HSA-RVT NPs showed the higher cellular uptake and cell inhibition rates. In vivo data showed that RGD-HSA-RVT NPs have good tumor enrichment characteristics and a significant difference in tumor inhibition, compared with the control group.

Conclusion: RGD-conjugated resveratrol HSA nanoparticles are an ideal drug delivery system, which can play a role in the treatment of ovarian cancer.

Keywords: resveratrol, HAS, nanoparticle, cellular uptake, cell viability, tissue distributions, pharmacokinetics

Introduction

Despite advances in treatment over the past 40 years, ovarian cancer is the second most common gynecological cancer, with more deaths than any other cancer of the reproductive system. Ovarian cancer is not easy to diagnose because the most common symptoms of persistent abdominal distension – pain and pelvic pressure – can be attributed to many reasons.[1] Patients may be asymptomatic before an abdominal mass or tumor metastasis is found in routine pelvic examination. Therefore, for most of the women who visit the hospital, it has advanced to the late stage before diagnosis.[2] About 75% of patients are in Phase II–IV at the time of diagnosis.[3] In the past two decades, chemotherapy for ovarian cancer has made great progress. The treatment for advanced disease has shifted from the use of alkylating agents to the currently recommended treatment based on taxane and platinum compounds.[1,3]

Resveratrol (RVT) is a non-flavonoid polyphenol containing stilbene structural elements, which is widely found in grapes, lilies and other plants.[4] RVT has been proved to have anti-inflammatory, anti-microbial, anti-oxidation, anti-virus, anti-atherosclerosis, immunomodulatory and neuroprotective effects. It is worth noting that the accumulated evidence supports that RVT has significant antitumor

Correspondence: Weipei Zhu
Email weipeizhu@163.com

submit your manuscript | www.dovepress.com
DovePress
http://doi.org/10.2147/DDDT.S248950

properties for a variety of human cancers, and many signaling pathways have been revealed, contributing to the anti-proliferation and apoptosis induced by RVT in mechanism. RVT has a significant therapeutic effect on hepatocellular carcinoma, ovarian carcinoma and leukemia. It was initially found to inhibit the invasion of hepatoma cells independent of its anti-proliferative activity.[5] Opipari et al reported on RVT induced autophagocytosis in ovarian cancer cells.[6] The chemopreventive effect of RVT on promyelocytic leukemia cells was first revealed by Jang et al.[7] Subsequent investigations elucidate the potential of RVT in inducing cell apoptosis in ovarian cancer cells.[8] It is necessary to point out that the addition of some cosolvent, such as polyoxyethylated castor oil, to traditional formulation to increase the solubility of RVT is related to severe and sometimes fatal hypersensitivity reactions.[9,10] To reduce the risk of hypersensitivity reactions with solvent-based formulation, patients are routinely pretreated with corticosteroids and antihistamines.

In order to overcome these obstacles, researchers are committed to improving the efficacy of drugs through pharmaceutical methods. Nanomaterials (NMs), including nanoparticles (NPs), micelles, dendrimers and liposomes, have become new tumor diagnostic probes and/or therapeutic drugs.[11–13] Abraxane® represents a successful clinical application of NMs in cancer nanomedicine. It is an albumin binding paclitaxel NP approved by FDA for the treatment of breast cancer,[14] non-small-cell lung cancer[15] and other solid tumors.[16,17]

In addition, ovarian cancer is one of the solid tumors outside of the current indications in which albumin-bound paclitaxel is an NCCN-recommended treatment option.[18] Adding paclitaxel of albumin into NPs makes hydrophobic paclitaxel water-soluble and avoids the use of solubilizer.[19] Through the EPR effect, Abraxane® could be accumulated in specific tumor sites, reducing its cytotoxicity to normal tissues and increasing its maximum tolerance dose.

Although albumin nanoparticles have excellent biological characteristics as drug carriers, it is still necessary to further study how to optimize their selective targeting ability to tumor cells and to release chemotherapy drugs in a controlled way. To solve the problem of site-specific targeting, some researchers have tried to couple the albumin drug carrier with targeted agents such as folic acid and transferrin to enhance its tissue specificity.[20–22]

Ideally, if a targeted agent with therapeutic effect could be physically or covalently bound to albumin, the therapeutic effect would be better. The arginine-glycineaspartic acid (RGD) sequence was found in fibronectin some 20 years ago as a cell attachment site. It was found that RGD peptides could inhibit tumor metastasis and induce cell apoptosis.[22–24] Since then, peptides containing RGD motif have been widely used to study the effects of RGD integrin interaction on cell adhesion, migration, growth and apoptosis. Integrin avβ3 is expressed on many kinds of tumor cells, including ovarian cancer.[25]

In this study, we prepared RGD-HSA-RVT NPs that had both good water solubility and tumor-targeting property. The generated NPs were characterized for physicochemical properties, the stability and in vitro release. Finally, comparison between RVT injection, HSA-RVT NPs and RGD-HSA-RVT NPs regarding tissue distributions and pharmacokinetics were also carried out using mice as the animal models.

Materials and Methods

Materials

RVT was gifted by Gaoyuan Biopharmaceuticals Co Ltd (Xian, China). RGD peptide (MW =1100 Da) was purchased from Biochempartner (Shanghai, China). SKOV3 ovarian cancer cell lines were purchased from the Shanghai Institute of Biochemistry and Cell Biology. The chemical and solvents used were analytical or HPLC. In this study, deionized water was used. Balb/c mice (5–6 weeks old, 22±2 g) were obtained from the Laboratory Animal Center of Faculty at the Second Affiliated Hospital of Soochow University, China. All animals were free of pathogens and had free access to food and water. Animal experiments were carried out in accordance with the guidelines issued by the National Institutes of Health and approved by the second affiliated hospital of Soochow University.

Preparation of RGD-HSA-RVT NPs

The RVT-HSA-NPs were prepared by a high-pressure homogenizer and emulsion-solvent evaporation method using. The initial concentration of HSA was 10 mg/mL in 10 mL deionized water. A mixture of chloroform and ethanol was added to the initial HSA solution at the ratio of 94:6 (5% v/v). RVT (1 mg/mL) was dissolved in a mixture of 5% v/v chloroform and ethanol (94:6), and then mixed with the HSA solution by volume. This emulsion was first homogenized for 2 min before being treated by a hand-held Omni Micro homogenizer, followed by

high-pressure homogenization. A homogenization pressure of 15,000 psi was applied to the emulsion, and 10 homogenization cycles were performed. The emulsion subjected to various homogenization cycles was passed through the homogenizer valve and collected through a connecting tube at the base of the assembly to form nano-sized emulsion droplets. After high-pressure homogenization, the obtained colloidal solution was transferred to a round bottom flask, and a vacuum pressure of 400 mm Hg was applied at 40 °C for 30 minutes with rotated evaporation at 90 rpm. This process ensured the complete removal of the organic solvent from the emulsion, resulting in the formation of RVT-HSA-NPs.

To conjugate RGD peptide to RVT-HSA-NPs, RVT-HSA -NPs modification with MBS (Methyl methacrylate-Butadiene-Styrene) was performed as described by Masahiro Tomita.[26] RVT-HSA-NPs were activated for half an hour at room temperature with MBS (10 mg/mL in DMF, heterobiofunctional cross-linker). After activation, the suspension and RGD peptide were co-incubated at room temperature for 3 h at a molar ratio of 10:1. In this step, the maleimide group of MBS reacted with the free sulfhydryl group of the Cys residue on the peptide. The reaction mixture was then dialyzed against PBS (pH 7.2) at 4°C overnight.

Physicochemical Characterization

Intensity-mean particle size and ζ-potential of NGs were determined using a Zetasizer NanoZS (Malvern Instruments Ltd.). All measurements were performed under automatic mode at 25°C. Software provided by the manufacturer was used to calculate the mean particle size (PS), the polydispersity index (PDI) and the ζ-potential of NGs. All measurements were performed at least in triplicate to calculate the mean values ± SD. Morphological examination of NPs was performed using transmission electronic microscopic (TEM, Philips CM120, Netherlands).

Drug-loading coefficient (DL%) and encapsulation ratio (ER%) were calculated as described earlier. Firstly, RVT was extracted from the RGD-HSA-NPs with 1 mL chloroform and ethanol mixture (94:6), and the extracted solution was then properly diluted prior to HPLC analysis. The content of RVT in the NPs was determined by the HPLC method described below. DL% and ER% were calculated according to Eq. (1) and Eq. (2):

$$DL\% = W_M/(W_P + W_M) \times 100 \quad (1)$$

$$ER\% = W_M/W_F \times 100 \quad (2)$$

where W_P is the weight of initial feeding polymer, W_M is the weight of drug incorporated in NPs, and W_F is the weight of initial feeding drug.

In the stability study, a sealed bottle of freshly prepared freeze-dried RGD-RVT-HSA-NPs was placed in a stability chamber and maintained at 25 °C and 60% RH. The PS, ζ-potentials, DL% and ER% of the samples were analyzed over a three-month period.

Drug Release Study

The release behaviors of RVT in HAS-NPs were investigated in PBS buffer with a pH value of 7.4. In order to maintain the sink conditions, Tween 80 (0.3%, w/v) was dissolved in the release medium (PBS, pH 7.4). RVT-HSA NPs and RGD-RVT-HSA NPs (10 mg) were dispersed in distilled water (0.15 mL) and loaded into a dialysis tube with a molecular weight of 14 kDa. That tube was then immersed in the release medium (30 mL) and incubated at 37 °C with 50 rpm. At 2, 4, 8, 12, 24, 48, 72, 96 and 120 h, the release medium (0.2 mL) was collected and replaced by a fresh medium (0.2 mL). The amount of RVT released from NPs was calculated by HPLC.

Cellular Uptake

The SKOV3 ovarian cancer lines were seeded into 24-well plates at a density of 1×10^6 cells/mL. After 24 h, each well was incubated with 1 mL coumarin-6-loaded free RVT, coumarin-6-loaded RVT-HSA NPs and coumarin-6-loaded RGD-RVT-HSA NPs (equivalent to 0.1 μg/mL of coumarin-6) for 2 h. In order to carry out quantitative analysis, the suspension was removed in a specified period of time and the well was washed three times with 1000 μL cold PBS before 50 μL of 0.5% Triton X-100 was added to each pore for cell lysis. The fluorescence intensity of each sample well was measured by a microplate reader. The excitation wavelength was 465 nm and the emission wavelength, 502 nm. In the qualitative study, the cells were washed three times with cold PBS and immobilized with 4% paraformaldehyde for 20 min; then the cells were washed twice with cold PBS and observed through a confocal laser scanning microscope.

In vitro Cytotoxicity Studies

SKOV3 ovarian cancer cells were seeded in 24-well plates at a density of 1×10^6 cells/well. After 24 h of incubation in 5% CO_2 at 37 °C, the cells were incubated with blank NPs, free RVT, RVT-HSA NPs and RGD-RVT-HSA NPs at a RVT concentration range of 0.5 to 75 μM for 15 min in serum-free media. After 15 min, the treated medium

was removed, the cells were washed with fresh medium, and 100 μL complete medium was added to culture for a further 24 or 48 h. After incubation, the medium was removed and replaced with 50 μL serum-free medium and 10 μL cell titer blue solution. After incubation in 5% CO2 at 37 °C for 2 hours, cell viability was evaluated by measuring the fluorescence produced by resorufin at excitation of 550 and emission of 590. The cytotoxicity of blank NPs, free RVT, RVT-HSA NPs and RGD-RVT-HSA NPs was tested to confirm that the cytotoxicity was a result of RVT treatment.

Biodistribution and in vivo Imaging Studies

To evaluate the distribution of the modified and non-modified RVT NPs in the main organs and tumors after administration, a biodistribution study was carried out. For this reason, subcutaneous SKOV3 tumors were grown in mice. Once the tumors reached a volume of 50–150 mm^3, they were considered well established. The treatment groups comprised of free RVT, RVT-HSA NPs and RGD-RVT-HSA NPs. A single dose of each preparation, equivalent to 10 mg/kg RVT, was injected into the mice via the tail vein. At 0.5 h, 1 h, 2 h, 4 h, 8 h, and 12 h after injection, the animals were sacrificed by cervical dislocation. Their plasma (0.1 mL) and 0.5 g organs (tumor, heart, liver, spleen, lung and kidney) were removed and flushed with water for three times to remove the remaining blood.

The plasma was separated by 12,000 rpm centrifugation for 10 min. Tissue samples were processed using IKA T 10 basic with 1 mL of distilled water added, and the supernatant was obtained by centrifugation at 4000 rpm for 10 min. All specimens were stored at −20 ºC until use. The RVT concentration in plasma and other organs was determined by HPLC using a Gemini C_{18} column (50×2.0 mm i.d., 5.0 μm particle size), and resveratrol-$^{13}C_6$ was used as the internal standard. Ten microliter of internal standard (resveratrol-$^{13}C_6$ 20 ng/mL) was added into 100 μL organ homogenate and extracted with 3 mL ethyl acetate. The mixture was vortexed for 2 min, and then centrifuged at 12,000 rpm for 5 minutes. The supernatant was transferred to another centrifuge tube and dried under air stream at room temperature. The dry residue was then reconstituted with 50 μL of methanol, and the solution was centrifuged at 12,000 rpm for 10 minutes before 20 μL of the supernatant was injected into the HPLC system for analysis. Acetonitrile water (26:74) was used as the mobile phase for elution with a flow rate of 1 mL/min, a column temperature of 30 °C, and a detection wavelength of 306 nm. All sample preparations were conducted under yellow light, and opaque plastic ware used to avoid light exposure of the agent. This method was validated over a linear range from 10.0 to 10,000 ng/mL for RVT and resveratrol-$^{13}C_6$. Results of the validation study demonstrated good intra- and inter-assay accuracy (<11.9%) and precision (<7.8%) for both analytes.

Another batch of animals was selected to evaluate the in vivo imaging study. When the animal model was established, 200 μL of Fluorescent probe Dir-labeled (1 mg/kg) free RVT, RVT-HSA NPs and RGD-RVT-HSA NPs was injected into the tumor-bearing mice via the tail vein. After anesthesia, the IVIS imaging system was used to collect the whole body fluorescence images of mice at 12 h. The exposure time was set at 600 ms, and the fluorescence signal was collected at 780 nm. The fluorescence images of tumor, heart, liver, spleen, lung and kidney were also collected.

Tumor Growth Inhibition Studies

The purpose of this study was to evaluate the antitumor ability of RVT NPs in ovarian cancer model. With this in mind, we established subcutaneous SKOV3 tumor model in nude mice. Once the tumor grew to a volume of 50 to 150 mm^3, the animals were randomly divided into groups so that the initial mean tumor volume was consistent across all groups. The comparison groups were blank NPs, free RVT, RVT-HSA NPs and RGD-RVT-HSA NPs. The mice in the treatment group were given 1 mL of each preparation, which was equivalent to 2 mg/kg RVT, via the tail vein. The doses were given everyday for one week, and the tumors were monitored for their growth and measured every third day. Tumor volumes were estimated as $V\ (mm^3) = (\text{length} \times \text{width}^2)/2$. The body weight was monitored throughout the study to detect signs of RVT toxicity. When the control tumor reached 1000 mm^3, the study stopped and the mice were sacrificed with the method of drowning.

Statistical Analysis

All experiments were repeated at least three times, and the experimental data are shown as mean± standard deviation (SD). Two tailed *t*-test and ANOVA were used to analyze the experimental data.

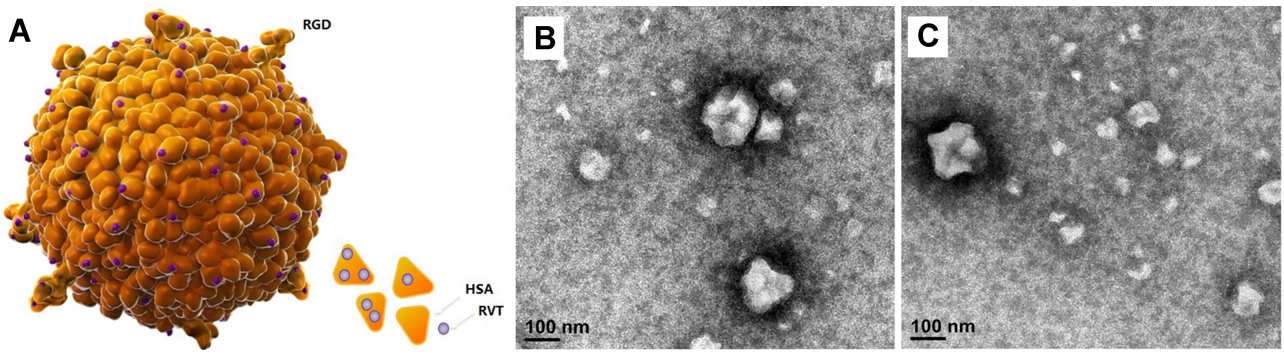

Figure 1 (**A**) The basic structure of RGD-RVT-HSA NPs. The transmission electron microscope of RGD-RVT-HSA NPs (**B**) and RVT-HSA NPs (**C**). (Magnification ×100,000).

Results

Characterization of RGD-RVT-HSA NPs

In this study, we used the emulsion-solvent evaporation method to prepare RGD-RVT-HSA NPs. NPs with smooth surfaces, good dispersion and relatively uniform size distributions were selected. The mean PS was 128.2 nm and the ζ-potentials was −21.42 mV. To modify HSA-NPs with RGD peptide, HSA-NPs suspension was pre-incubated with MBS. The activated HSA-NPs were then incubated with RGD peptide. Transmission electron micrographs showed that RGD peptide-conjugated HSA-NPs have irregular surface, good dispersion (PDI=0.132±0.045) and a uniform size distribution (Mean PS=128.2±11.56 nm). Conjugated and non-conjugated nanoparticles were then observed by TEM (Figure 1). The other parameters are shown in Table 1. In addition, according to the stability data, the RGD-RVT-HSA NPs can be preserved stably during the observation period.

Drug Release Study

In vitro release of RVT from the NPs was investigated. Figure 2 shows the release profile of four different NPs groups. Compared with the rapid release of free RVT, the two NPs groups exhibited sustained release in a similar manner and an initial burst release (RVT-HSA NPs 42.3% and RGD-RVT-HSA NPs 37.5%) was also observed. The RGD-modified RVT-HSA NPs had a slightly more sustained release effect than the unmodified NPs. The release curve shows that the samples for the stability test did not change the drug release characteristics.

Cellular Uptake

In order to study the selectivity and internalization of NPs, we examined the uptake of different NPs in SKOV3 cells. As shown in Figure 3, the fluorescence intensity of free RVT was the lowest observed among the three formulations and that of RVT-HSA NPs was higher. However, RGD-RVT-HSA NPs uptake was significantly higher than that of RVT-HSA NPs (approximately 3.6-fold higher), which might be the result of the targeting capacity of integrin receptors expression in SKOV3 cells. The results of cellular uptake could be related to the expression levels of integrin on cell surface, indicating that the RGD motif could recognize and target integrin receptors on cell surface.

In vitro Cytotoxicity Studies

In order to evaluate the antiproliferative effect of different RVT preparations, the SKOV3 cells were analyzed by MTT after 24 or 48 hours of treatment (Figure 4). With the increase of culture time and RVT concentration, the viability of

Table 1 Characterization of the Prepared RVT-HSA NPs

Formulation	Time (m)	Mean PS (nm)	PDI	ζ-Potential (mV)	RVT	
					DL%	ER%
RVT-HSA NPs	0	118.3±9.77	0.143±0.051	−26.71±5.53	6.5±1.45	79.8±5.87
RGD-RVT-HSA NPs	0	128.2±11.56	0.132±0.045	−21.42±4.56	7.6±1.39	83.6±6.34
	1	125.6±12.71	0.136±0.072	−23.54±5.52	7.4±1.44	82.4±5.78
	3	123.8±12.89	0.138±0.082	−25.36±6.16	7.1±1.27	82.3±5.19

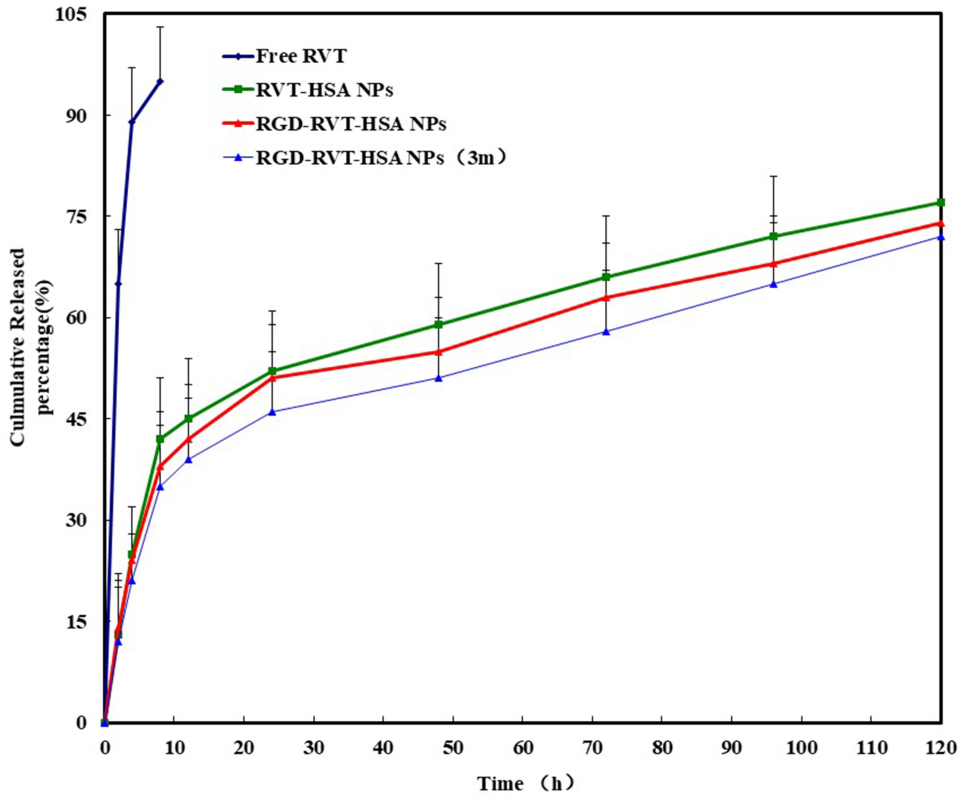

Figure 2 Cumulative drug release (mean ± SD %, n = 6) profiles of free RVT, RVT-HSA NPs, RGD-RVT-HSA NPs and RGD-RVT-HSA NPs (3m) over time intervals of 2, 4, 8, 12, 24, 48, 72, 96, and 120 h.

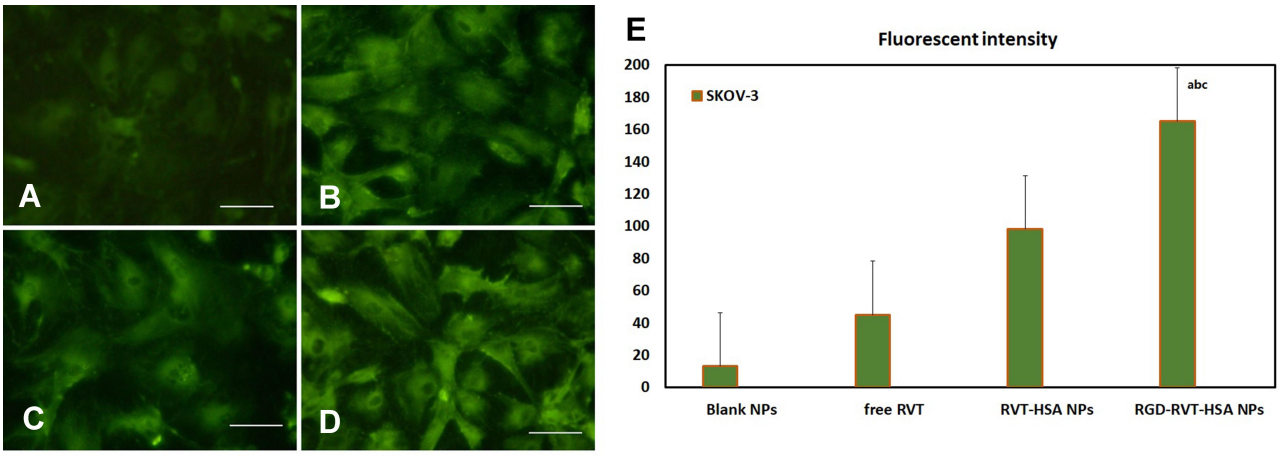

Figure 3 Confocal images of cellular uptake of blank NPs (**A**), free RVT (**B**), RVT-HSA NPs (**C**), RGD-RVT-HSA NPs (**D**) by SKOV-3 cells. Incubation time was 2 hours. (**E**) Fluorescence intensity of four groups. [a]p < 0.05, compared with blank NPs; [b]p < 0.05, compared with free RVT; [c]p < 0.05, compared with RVT-HSA NPs.

SKOV3 cells decreased. With the overexpression of αvβ3 integrin in SKOV3 cells, NPs combined with RGD showed higher toxicity (32% cell viability at 24 h and 15% cell viability at 48 h). In the experiment of cell viability, free RVT, RVT-HSA NPs and RGD-RVT-HSA NPs showed time- and dose-dependent cytotoxic activity on SKOV3 cells. It is worth noting that RGD-RVT-HSA NPs achieved the lowest cell viability among all three formulations at all equivalent drug concentration levels.

Biodistribution and in vivo Imaging Studies

A biodistribution study was performed to investigate the distribution of modified and non-modified RVT NPs in vivo. As

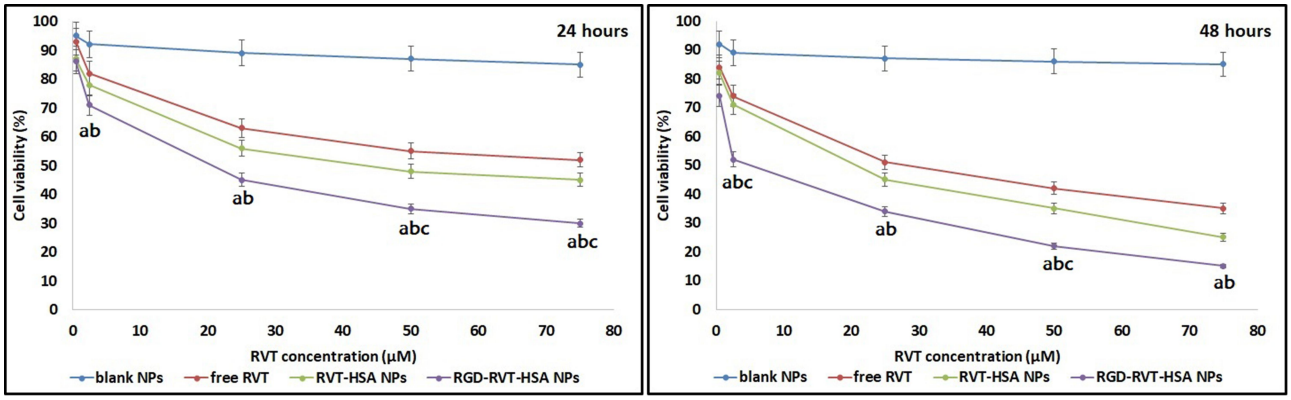

Figure 4 Effect of different RVT formulations on cell death in SKOV3 cancer cells. Assessment of cell viability of SKOV3 cells treated with free RVT, RVT-HSA NPs and RGD-RVT-HSA NPs at RVT concentration of 0.5–75 μM for 15 min followed by 24 or 48 h incubations. [a]$p < 0.05$, compared with blank NPs; [b]$p < 0.05$, compared with free RVT; [c]$p < 0.05$, compared with RVT-HSA NPs.

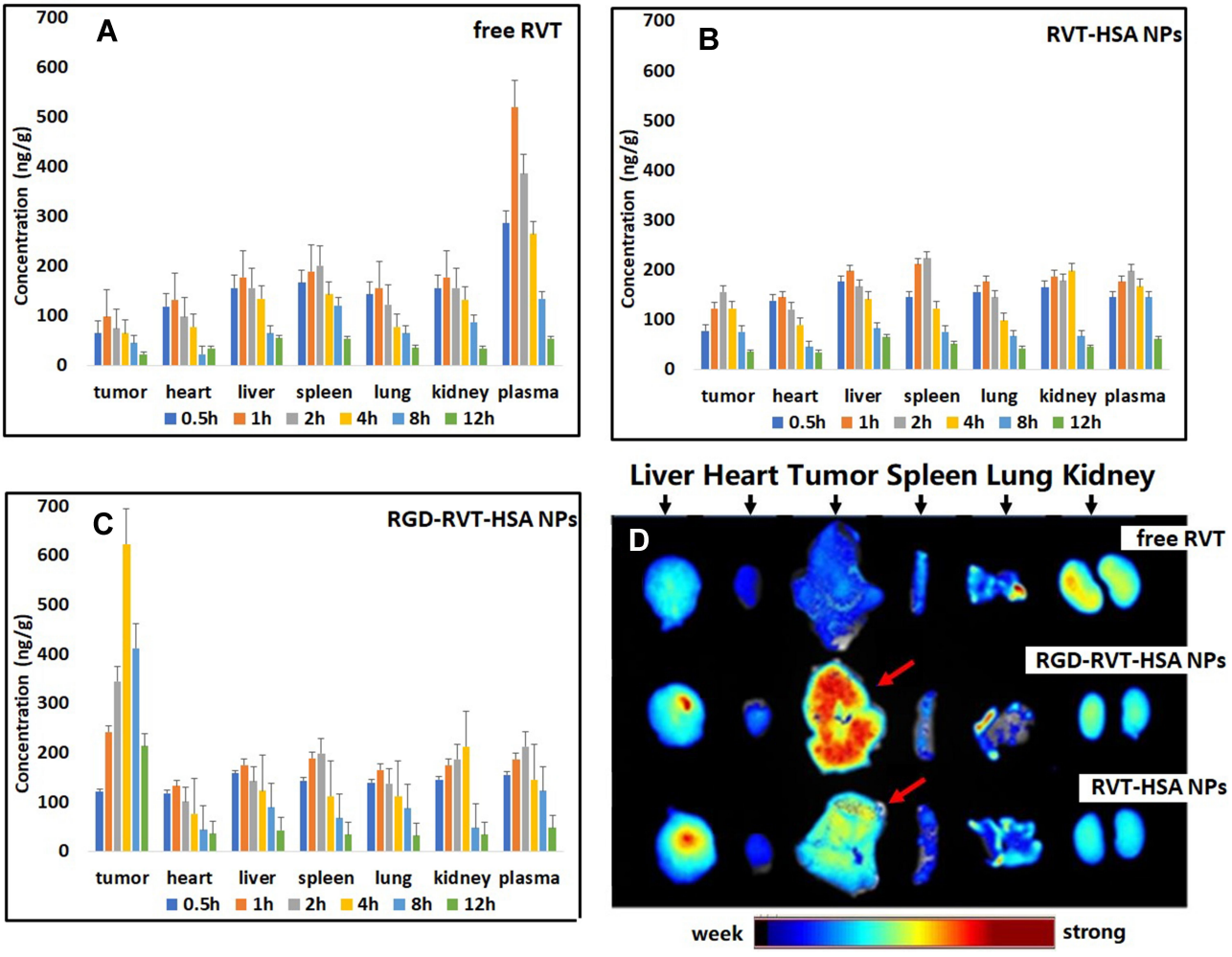

Figure 5 The research results of tissue distribution and in vivo imaging studies. (**A**) free RVT, (**B**) RVT-HSA NPs, (**C**) RGD-RVT-HSA NPs and (**D**) Fluorescence images of three groups (at 12 h).

shown in Figure 5A, in the group of free RVT, plasma drug concentration peaked at 1h and was then rapidly eliminated with no selective accumulation in any tissue. In both free RVT and RVT-HSA NPs, the distribution of RVT in vivo was relatively balanced and there was no obvious organ accumulation (Figure 5B). Levels of RVT distribution in tumor were limited for two groups. As for RGD-RVT-HSA NPs, the distribution of the drug in different tissues varied significantly. It accumulated in higher quantities in tumors compared to the other treatment groups. RVT concentration in mice tumor (623 ng/g, 4 hrs) in the RGD-RVT-HSA NPs group was significantly higher than that in other tissues and the plasma (Figure 5C). RVT showed the highest value of AUC (4672.3 ngh/g) and target index (TI) in tumor, and the difference was statistically significant ($p<0.05$). The TIs of different formulations are listed in Table 2. This phenomenon of tumor enrichment may be attributable to the receptor-mediated mechanism, which may bring benefits to clinical treatment. Meanwhile, Figure 5D shows that after being given near-infrared probe Dir 12h and examined by organ imager, RGD-RVT-HSA NPs had stronger fluorescence in the nude mouse's subcutaneous tumor site than in other groups. This result indicated that RGD-RVT-HSA NPs had obvious targeting effect on subcutaneous tumors, with a potential to actively deliver drugs to tumor tissues.

This result also showed that the RGD modified NPs had advantages in increasing RVT concentration in tumor sites and reducing its distribution in peripheral organs.

Tumor Inhibition Study

Through the tumor growth inhibition experiment, the therapeutic effect of different RVT preparations in vivo was evaluated. Compared with the control group and the free RVT treatment group, all RVT NPs groups showed inhibited tumor growth at the experimental dose. RGD-RVT-HSA NPs were most effective in controlling tumor growth throughout the 27-day study (Figure 6). The growth trends of the three groups were similar at the beginning of the study but changed half way through. From day 15, there was a significant difference in tumor volume between free RVT, RVT-HSA NPs and RGD-RVT-HSA NPs. At the end of the study, the tumor volumes were 823.6 ± 76.4 mm^3 for control group, 654.7 ± 78.2 mm^3 for Free RVT, 523.9 ± 52.4 mm^3 for RVT-HSA NPs and 345.7 ± 36.3 mm^3 for RGD-RVT-HSA NPs. The RGD-RVT-HSA NPs treatment was consistently more effective in controlling tumor growth than other treatments throughout the study. The mouse weights recorded throughout the study were fairly constant, indicating that the preparation was not significantly toxic.

Discussion

Many studies have shown that NPs loaded with chemotherapeutic drugs can be delivered into tumor cells and NPs accumulate passively in tumors in a nontargeted manner through the enhanced permeability and retention (EPR) effect. Ideally, it would be much better if a targeting agent could be physically conjugated to the surface of NPs, and delivers the vehicle through a target-way, which represents a potential approach to further enhance the antitumor efficacy. In this study, various key parameters crucial to the preparation of RVT-HSA NPs with a size of 100–200 nm were optimized using a high-pressure homogenizer.

As related products have been put on the market, the preparation parameters are easier to explore. The purpose of this study was to investigate the feasibility of binding RGD peptide to HAS-NPs. The integrins are a class of cell surface glycoproteins, which mediate cell survival, proliferation, and migration through explicit non-covalent interactions with endogenous extra cellular matrix (ECM) proteins. They are highly expressed in activated endothelial cells and solid tumor cells but rarely so in resting endothelial cells. Among members of the integrin family, integrin avβ3 plays an important role in tumor biology as well as tumor angiogenesis, apoptosis and metastasis. We have developed a novel carrier system based on HAS NPs, which could be modified by RGD peptides for targeting purposes.

Table 2 The AUC_{0-12h} of RVT in Plasma and Tissues After i.v. Administration of Injection and NPs to Mice (n=6)

Formulation	Tumor	Heart	Liver	Spleen	Lung	Kidney	Plasma
Free RVT (ng·h/g)	623.3*	669.8	1178.5	1506	901.3	1218.5	2482
RVT-HSA-NPs (ng·h/g)	1088.8*	839.8	1324	1304.8	1034.5	1400.5	1668.3
RGD-RVT-HSA NPs (ng·h/g)	4672.3	756	1194.8	1148	1112	1344	1520
Ratio[a]	7.5	1.1	1.0	0.8	1.2	1.1	0.6
Ratio[b]	4.3	0.9	0.9	0.9	1.1	1.0	0.9

Notes: [a]The ratio was AUC (RGD-RVT-HSA NPs)/AUC (Free RVT); [b]The ratio was AUC (RGD-RVT-HSA NPs)/AUC (RVT-HSA-NPs); *P<0.05: vs AUC (RGD-RVT-HSA NPs).

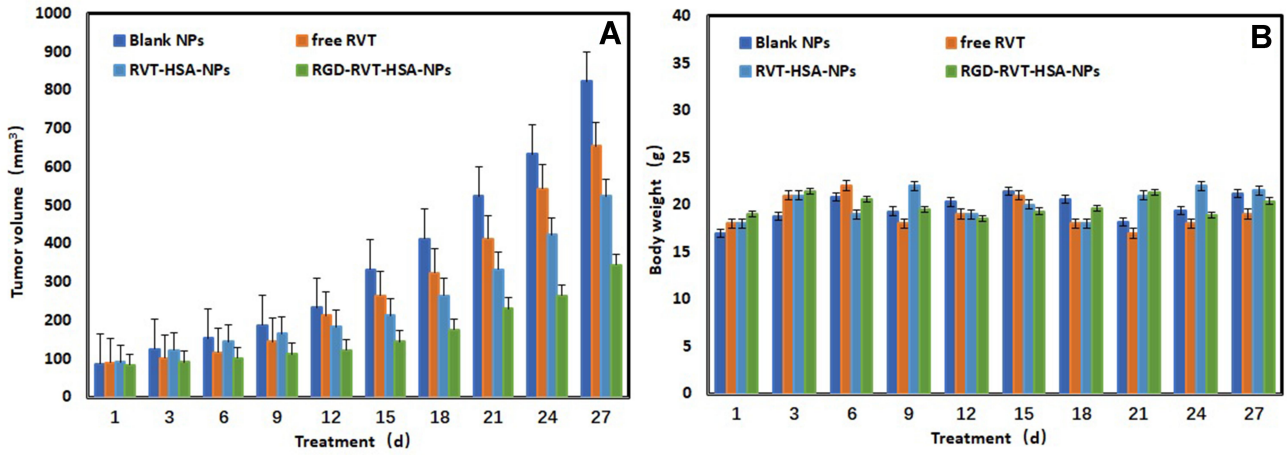

Figure 6 Changes of tumor volume (**A**) and body weight (**B**) in nude mice transplanted with SKOV3 cancer cells of blank NPs, free RVT, RVT-HSA NPs and RGD-RVT-HSA NPs.

The in vitro drug release of RVT from the HSA-NPs has been studied and the method of in vitro drug release has previously been confirmed in the literature.[27] The NPs were dispersed in PBS at 37°C and in shaking conditions in order to simulate the dynamic in vivo conditions. The results were similar to other nano preparations, showing an initial burst release and consistency in in vitro drug release.[28] For example, the NPs prepared in the two studies had similar particle sizes and manners of release.[29] Rather than completely releasing the drug within 24 hours, it allowed continuous targeting of the cancer cells with a decrease in cell viability over time. The main reason for the initial burst release is that the drug on the surface of NPs was released into the medium first and then into the core of NPs. Since the modification of RGD did not affect the spatial structure of NPs, there was no significant difference in the release curves between modified and non-modified NPs. At the same time, it has been reported that the use of albumin carrier platform can enhance the anti-tumor effect of drugs in ovarian cancer.[30] This also makes the results of this study hopeful for further clinical application.

Acknowledgments

This work is supported by the maternal and child health research project of Jiangsu province (F201709) and the maternal and child health key talents of Jiangsu province (FRC201714).

Disclosure

The authors report no conflicts of interest for this work.

References

1. Lister-Sharp D, McDonagh MS, Khan KS, Kleijnen J. A rapid and systematic review of the effectiveness and cost-effectiveness of the taxanes used in the treatment of advanced breast and ovarian cancer. *Health Technol Assess*. 2000;4(17):1–113. doi:10.3310/hta4170
2. Memarzadeh S, Berek JS. Advances in the management of epithelial ovarian cancer. *J Reprod Med*. 2001;46(7):621–629.
3. Beers MH, Berkow R, editors. Ovarian cancer. In: *The Merck Manual of Diagnosis and Therapy*. 17th. Hitehouse Station, NJ: Merck Research Laboratories; 1999:1962–1964.
4. Nawaz W, Zhou Z, Deng S, et al. Therapeutic versatility of resveratrol derivatives. *Nutrients*. 2017;9(11):1188. doi:10.3390/nu9111188
5. Kozuki Y, Miura Y, Yagasaki K. Resveratrol suppresses hepatoma cell invasion independently of its anti-proliferative action. *Cancer Lett*. 2001;167(2):151–156. doi:10.1016/S0304-3835(01)00476-1
6. Opipari AW, Tan L, Boitano AE, Sorenson DR, Aurora A, Liu JR. Resveratrolinduced autophagocytosis in ovarian cancer cells. *Cancer Res*. 2004;64(2):696–703. doi:10.1158/0008-5472.CAN-03-2404
7. Jang M, Cai L, Udeani GO, et al. Cancer chemopreventive activity of resveratrol, a natural product derived from grapes. *Science*. 1997;275(5297):218–220. doi:10.1126/science.275.5297.218
8. Gwak H, Kim S, Dhanasekaran DN, Song YS. Resveratrol triggers ER stress-mediated apoptosis by disrupting N-linked glycosylation of proteins in ovarian cancer cells. *Cancer Lett*. 2016;371(2):347–353. doi:10.1016/j.canlet.2015.11.032
9. Gelderblom H, Verweij J, Nooter K, Sparreboom A. Cremophor EL: the drawbacks and advantages of vehicle selection for drug formulation. *Eur J Cancer*. 2001;37(13):1590–1598. doi:10.1016/S0959-8049(01)00171-X
10. Ten Tije AJ, Verweij J, Loos WJ, Sparreboom A. Pharmacological effects of formulation vehicles: implications for cancer chemotherapy. *Clin Pharmacokinet*. 2003;42(7):665–685. doi:10.2165/00003088-200342070-00005
11. Emerich DF. Nanomedicine-prospective therapeutic and diagnostic applications. *Expert Opin Biol Ther*. 2005;5(1):1–5. doi:10.1517/14712598.5.1.1
12. Wagner V, Dullaart A, Bock AK, Zweck A. The emerging nanomedicine landscape. *Nat Biotechnol*. 2006;24(10):1211–1217. doi:10.1038/nbt1006-1211
13. Nie S, Xing Y, Kim GJ, Simons JW. Nanotechnology applications in cancer. *Annu Rev Biomed Eng*. 2007;9:257–288. doi:10.1146/annurev.bioeng.9.060906.152025

14. Miele E, Spinelli GP, Tomao F, Tomao S, Tomao S. Albumin-bound formulation of paclitaxel (Abraxane ABI-007) in the treatment of breast cancer. *Int J Nanomedicine*. 2009;4:99–105. doi:10.2147/ijn.s3061
15. Green MR, Manikhas GM, Orlov S, et al. Abraxane, a novel Cremophor-free, albumin-bound particle form of paclitaxel for the treatment of advanced non-small-cell lung cancer. *Ann Oncol*. 2006;17(8):1263–1268. doi:10.1093/annonc/mdl104
16. Gradishar WJ. Albumin-bound paclitaxel: a next-generation taxane. *Expert Opin Pharmacother*. 2006;7(8):1041–1053. doi:10.1517/14656566.7.8.1041
17. Stinchcombe TE, Socinski MA, Walko CM, et al. Phase I and pharmacokinetic trial of carboplatin and albumin-bound paclitaxel, ABI-007 (Abraxane) on three treatment schedules in patients with solid tumors. *Cancer Chemother Pharmacol*. 2007;60(5):759–766. doi:10.1007/s00280-007-0423-x
18. NCCN Clinical Practice Guidelines in Oncology. Ovarian cancer including fallopian tube cancer and primary peritoneal cancer. V1; 2015. Available from: http://www.nccn.org/professionals/physician_gls/pdf/ovarian.pdf. Accessed March 16, 2015.
19. Damascelli B, Cantu G, Mattavelli F, et al. Intraarterial chemotherapy with polyoxyethylated castor oil free paclitaxel, incorporated in albumin nanoparticles (ABI-007): phase I study of patients with squamous cell carcinoma of the head and neck and anal canal: preliminary evidence of clinical activity. *Cancer*. 2001;92(10):2592–2602. doi:10.1002/1097-0142(20011115)92:10<2592::aid-cncr1612>3.0.co;2-4
20. Zhang L, Hou SX, Mao SJ, Wei DP, Song XJ, Lu Y. Uptake of folate-conjugated albumin nanoparticles to the SKOV3 cells. *Int J Pharm*. 2004;287(1–2):155–162. doi:10.1016/j.ijpharm.2004.08.015
21. Ulbrich K, Hekmataraa T, Herberta E, Kreuter J. Transferrin- and transferrin-receptor-antibody-modified nanoparticles enable drug delivery across the blood–brain barrier (BBB). *Eur J Pharm Biopharm*. 2009;71(2):251–256. doi:10.1016/j.ejpb.2008.08.021
22. Anuradha CD, Kanno S, Hirano S. RGD peptide-induced apoptosis in human leukemia HL-60 cells requires caspase-3 activation. *Cell Biol Toxicol*. 2000;16(5):275–283. doi:10.1023/A:1026758429238
23. Madeja Z, Sroka J. Contact guidance of Walker carcinosarcoma cells by the underlying normal fibroblasts is inhibited by RGD-containing synthetic peptides. *Folia Histochem Cytobiol*. 2002;40(3):251–260.
24. Kang IC, Kim DS, Jang Y, Chung KH. Suppressive mechanism of salmosin, a novel disintegrin in B16 melanoma cell metastasis. *Biochem Biophys Res Commun*. 2000;275(1):169–173. doi:10.1006/bbrc.2000.3130
25. Cannistra SA, Ottensmeier C, Niloff J, Orta B, DiCarlo J. Expression and function of β1 and avβ3 integrins in ovarian cancer. *Gynecol Oncol*. 1995;58(2):216–225. doi:10.1006/gyno.1995.1214
26. Tomita M, Sugi H, Ozawa K, Tsong TY, Yoshimura T. Targeting antigen-specific receptors on B lymphocytes to generate high yields of specific monoclonal antibodies directed against biologically active lower antigenic peptides within presenilin 1. *J Immunol Methods*. 2001;251(1–2):31–43. doi:10.1016/S0022-1759(01)00299-X
27. Nam S, Lee SY, Kang WS, Cho HJ. Development of resveratrol-loaded herbal extract-based nanocomposites and their application to the therapy of ovarian cancer. *Nanomaterials (Basel)*. 2018;8(6):pii: E384. doi:10.3390/nano8060384
28. Zhao D. Preparation, characterization, and in vitro targeted delivery of folate-decorated paclitaxel-loaded bovine serum albumin nanoparticles. *Int J Nanomed*. 2010;5:669–677.
29. Geng T, Zhao X, Ma M, Zhu G, Yin L. Resveratrol-loaded albumin nanoparticles with prolonged blood circulation and improved biocompatibility for highly effective targeted pancreatic tumor therapy. *Nanoscale Res Lett*. 2017;12(1):437. doi:10.1186/s11671-017-2206-6
30. Noorani L, Stenzel M, Liang R, Pourgholami MH, Morris DL. Albumin nanoparticles increase the anticancer efficacy of albendazole in ovarian cancer xenograft model. *J Nanobiotechnology*. 2015;13:25. doi:10.1186/s12951-015-0082-8